applied sciences

MDPI

Article

Experimental Study of the Effect of High Temperature on the Mechanical Properties of Coarse Sandstone

Sijiang Wei [1,2], Yushun Yang [3,*], Chengdong Su [1,2], Syabilla Rachmadina Cardosh [1] and Hao Wang [1]

1 School of Energy Science and Engineering, Henan Polytechnic University, Jiaozuo 454010, China; jzitwsj@126.com (S.W.); sucd@hpu.edu.cn (C.S.); syabi@outlook.co.id (S.R.C.); wang979697227@163.com (H.W.)
2 Collaborative Innovation Center of Coal Work Safety, Henan Province, Jiaozuo 454000, China
3 College of Resources and Environmental Science, Chongqing University, Chongqing 400044, China
* Correspondence: 20152001005@cqu.edu.cn

Received: 7 May 2019; Accepted: 10 June 2019; Published: 14 June 2019



Featured Application: In order to study the effect of high temperature on mechanical properties of coarse sandstone, uniaxial and triaxial compression tests of coarse sandstone specimens at different temperatures were carried out. It is considered that with the increase of temperature, the temperature damage factor increases gradually, and the longitudinal wave velocity decreases gradually; 500 °C is the temperature threshold of coarse sandstone specimens under uniaxial compression. The actual fracture angle of coarse sandstone specimen under triaxial compression is basically the same as the theoretical calculation value, and the actual fracture angle is negatively correlated with the confining pressure.

Abstract: In order to study the effect of high temperature on the mechanical properties of rock, two groups of coarse sandstone samples were subjected to the uniaxial compression and triaxial compression test at room temperature of 25 °C and high temperatures of 100~1000 °C. The study comes to some conclusions: (1) With the increase of temperature, the longitudinal wave velocity gradually decreases, and the damage factor of temperature gradually increases. (2) For uniaxial compression tests at different temperatures, the high temperature action within 500 °C has a strengthening effect on the compression strength, and the high temperature effect has a weakening effect on the compression strength when temperatures exceed 500 °C; so 500 °C is the temperature threshold. (3) For triaxial compression tests at different temperatures, the rock strength is positively correlated with temperature and confining pressure when the temperature is lower than 800 °C and the confining pressure is lower than 15 MPa; the rock strength is negatively correlated with temperature and confining pressure when the temperature is over 800 °C and confining pressure is above 15 MPa, so 800 °C is the temperature threshold, and 15 MPa is the confining pressure threshold. (4) In the triaxial compression, the actual fracture angle of the sample after high temperature is basically the same as the theoretical calculation value, high temperature has little effect on the actual fracture angle of the sample, and the actual fracture angle is negatively correlated with the confining pressure.

Keywords: high temperature; uniaxial compression; triaxial compression; strength properties; deformation properties

1. Introduction

With the development of nuclear waste disposal, underground coal gasification, geothermal resource, coal mine gas explosion, underground engineering, fire reconstruction, and high temperature

rock mechanics have become some of the most difficult problems to be solved. A lot of experimental studies and theoretical discussions on physical and mechanical parameters of rock were done by domestic and foreign scholars, which include the deformation mechanism, rock failure criterion, constitutive relation, and thermal cracking and rock damage mechanism under high temperature.

He et al. [1] studied the fracture density and cracking mechanism of sandstone after high temperature. Zuo et al. [2,3] investigated the variation of characteristic parameters such as fracture toughness, elastic modulus, and ductility ratio with the three-point bending test of sandstones on different temperatures. Wu et al. [4–6] studied the mechanical properties and acoustic emission of sandstone and granite after high temperature. You et al. [7] studied the mechanical properties and the longitudinal wave velocity of coarse sandstone after high temperature. Chen et al. [8] believed that as the heating temperature increases, the peak stress and elastic modulus of heated granite decreases, while the peak strain increases. For a heating temperature below 400 °C, the effects of temperature on peak stress, elastic modulus, and the peak strain of granite are relatively small. Brotóns et al. [9] studied the effect of high temperatures in the physical and mechanical properties of a calcarenite (San Julian's stone). Huang et al. [10] studied the effect of heat treatment on the dynamic compressive strength of Longyou sandstone. Xu et al. [11] used an MTS810 electro-hydraulic servo material system and MTS652.02 high temperature environment furnace to test the compression of granite under different loading rates at real-time high temperature. Based on the experimental data, Yao et al. [12] established an empirical equation to relate the dynamic tensile strength of LS to the loading rate and the heat-treatment temperature. Yu et al. [13] believed the evolution of permeability of the rock samples after cycles of freeze–thaw in a complete stress–strain process under triaxial compression is closely related to the variation of the microstructure in the rock. Chmel et al. [14] applied the acoustic emission technique for monitoring the high-speed cracking process in three kinds of impact-damaged granites at temperatures of 20–600 °C. Geng et al. [15] investigated the effect of high temperature on mechanical properties of concrete. Huang et al. [16] carried out uniaxial compression tests and acoustic wave tests on high temperature rock samples cooled by water, and analyzed the variation of peak strength, elastic modulus, attenuation coefficient, longitudinal wave velocity and main frequency of rock samples in different states. Su et al. [17–19] studied the deformation and mechanical properties of fine sandstone, coarse sandstone and weakly bonded medium sandstone under high temperature, and analyzed the mineral composition, structural characteristics, and the correlation between mechanical parameters and temperature of samples after high temperature. Huang et al. [20] carried out Brazilian splitting tests on granite disc patterns after high temperature, and obtained the variation law of tensile strength with temperature. Shao et al. [21] introduced the influence of temperature change on rock deformation characteristics and established improved elastic and viscous elements. Based on Burgers's rheological model, rock rheological equation under variable temperature field was deduced, and the corresponding theoretical solutions of creep equation, unloading equation and relaxation equation were deduced. Li et al. [22] carried out triaxial compression tests after high temperature and uniaxial compression tests under real-time high temperature. Typical stress–strain curves and acoustic emission characteristics under various test conditions were analyzed, and the damage Degradation Laws of strength and deformation parameters were studied comparatively. Kong et al. [23] studied the uniaxial compression tests of sandstone after different temperature treatments were conducted and the frequency–amplitude characteristics of AE signals. Becattinin et al. [24] investigated the six types of rocks of Alpine for their suitability for high-temperature packed-bed thermal energy storage. Zhang et al. [25] studied the influence of high temperature on mechanical properties and acoustic emission characteristics of gritstone, and the X-ray diffraction, uniaxial compression and acoustic emission tests were carried out on the gritstone after the high temperature of 200 °C to 800 °C. Ersoy et al. [26] investigated the engineering behaviors of rocks exposed to temperatures ranging from 200 to 1000 °C and changes in geo-mechanical properties, as well as related mineralogical changes, were examined. The above studies show that the changes of rock mechanical properties of different kinds of samples after high

temperature action have an obvious similarity. However, due to the differences in the history of rock formation, composition, and other factors, different rock types show some differences.

Sandstones are widely distributed and come with a wide variety and different types of sandstone are subject to the diagenetic history, which makes it different in shape, size, mineral composition, and cementation [17]. The heat resistance of different minerals is different under high temperature, and the complex physical and chemical reaction of these minerals under high temperature making its mechanical properties very different. Two groups of coarse sandstones are heated from 100 to 1000 °C, naturally cooled to the room temperature, and then uniaxial compression and triaxial compression tests were carried out in the RMT-150B rock mechanics test system to analyze the temperature and stress conditions. The research results provide some reference and help for the development of engineering design and high temperature rock mechanics theory.

2. Sample Preparation and High Temperature Treatment

2.1. Sample Preparation

The test samples were taken from the coarse sandstone of coal seam roof, and the rock blocks with a size larger than 200 mm were selected in the field, and the rock core was drilled by wet drilling method in the laboratory. A standard cylindrical sample with a diameter of 50 mm and a height of 100 mm was cut and polished, and the processing accuracy meets the requirements of the regulation [27]. We divided samples in two groups A and B according to macroscopical differences. Among them, 30 samples from group A are subject to uniaxial compression test, and 25 samples from group B are subject to uniaxial compression test. The density of group A is 22.75~24.10 kN/m^3, the average value was 23.46 kN/m^3, and the dispersion coefficient was 1.4%. The density of group B is 23.71~24.24 kN/m^3, the average value is 24.01 kN/m^3, and the dispersion coefficient is 0.41%. The sample showed no obvious defects such as joints and cracks, and the macroscopicity was relatively uniform.

2.2. High Temperature Treatment

Specimens were heated with °C resistance furnace, and its type is KSW-5D-12, which has an automatic temperature control module, carbon rod components and high-performance fiber insulation, the maximum temperature can reach 1200 °C. The temperature was set from 100 °C, 200 °C, 300 °C, 400 °C, 500 °C, 600 °C, 700 °C, 800 °C, 900 °C and 1000 °C at a heating rate of 10 °C/min except for the room temperature 25 °C. When the temperature of the sample was raised to the set temperature, the temperature is kept constant for 4 h, and then the samples are naturally cooled to room temperature in the furnace. The coarse sandstone samples after different temperatures are shown in Figures 1 and 2.



(**a**) 25 °C (**b**) 100 °C (**c**) 200 °C (**d**) 300 °C (**e**) 400 °C



(**f**) 500 °C (**g**) 600 °C (**h**) 700 °C (**i**) 800 °C (**j**) 900 °C

Figure 1. Group A samples at different temperature.

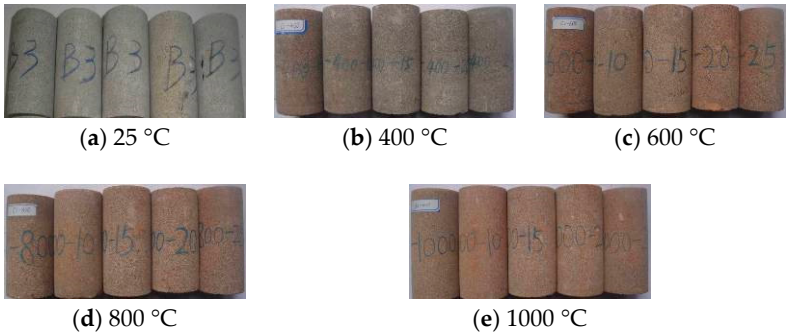

(**a**) 25 °C (**b**) 400 °C (**c**) 600 °C

(**d**) 800 °C (**e**) 1000 °C

Figure 2. Group B samples at different temperature.

It can be seen from Figures 1 and 2 that the apparent color of the sample changes after high temperature action, and the mineral composition of the two samples differs. The color of the samples in group A is grayish white at room temperature, it changes to dark brown after high temperature, and gradually turns into light pink, after high temperature of 100~500 °C, then it changes to brownish red after the temperature of 600~900 °C, and the higher the temperature is, the deeper the red will be. The color of the samples in group B is light white at room temperature, and it changes to dark brown red gradually after high temperature from 400 to 1000 °C, and the higher the temperature is, the more obvious the red color will be. There are no apparent cracks and disintegration in the two groups of samples after high temperature, and remained intact.

3. Testing Device and Scheme Design

3.1. Testing Device

3.1.1. Ultrasound Testing Device

The ultrasonic test of the sample uses the UTA2001A ultrasonic inspection monitor, Kefeng Electronic Instrument Factory, Nanyang, Henan Province, China. As shown in Figure 3. UTA2001A is an intelligent measuring instrument with a microprocessor. The whole operation of the instrument is under its control and management. The measured value, processing result and status information can be displayed on the picture tube of the detector. The instrument has the advantages of simple operation, convenience, complete function and high reliability. Its frequency response range is 1~500 kHz, acoustic time range is 9999.9 μs, acoustic time resolution is 0.1 μs, acoustic speed range is 9.999 km/s, emission voltage is divided into 300 V and 1000 V, attenuation range is 0~50 dB, minimum interval is 5 dB, sampling frequency is 10, 5, 2, 1 MHz, probe frequency is 12.5 kHz~500 kHz. The instrument adopts high-speed data acquisition and storage technology. Once the button is pressed, an ultrasonic signal waveform can be acquired. One signal can collect 2048 data points, and the measurement accuracy is high.



Figure 3. UTA2001A ultrasonic inspection monitor.

3.1.2. Mechanical Testing Device

The test device adopts the RMT-150B electro-hydraulic servo test system developed by the Wuhan Institute of Rock and Soil Mechanics of the Chinese Academy of Sciences, as shown in Figure 4. The maximum axial load of the test system is 1000 kN, the maximum horizontal load is 500 kN, and the maximum confining pressure is 50 MPa. It can carry out tests such as rock uniaxial compression, indirect (direct) stretching, compression-shear and triaxial compression tests. It can adopt various control modes of load, displacement, and stroke. During the test, the computer automatically collects a load and deformation and displays it in real time.

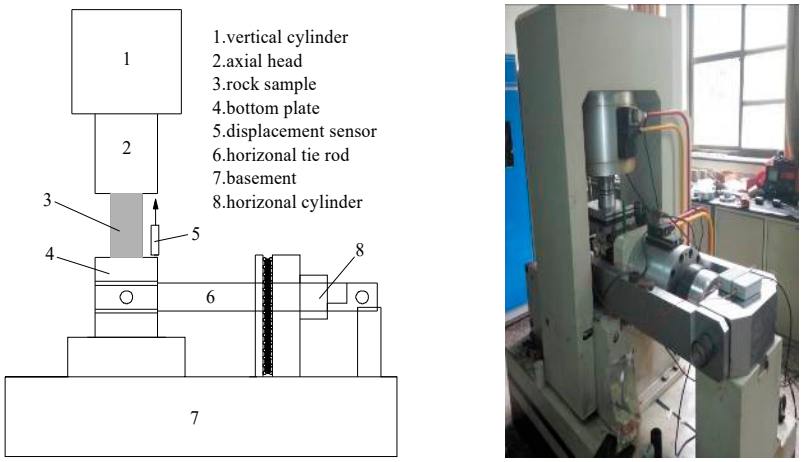

(**a**) Schematic diagram of uniaxial compression (**b**) Test symtem

Figure 4. Electro-hydraulic servo rock test system of RMT-150B.

3.2. Scheme Design

(1) All samples were tested for longitudinal wave velocity at room temperature 25 °C and after high temperature treatment using UTA-2000A non-metallic ultrasonic monitoring analyzer.

(2) The uniaxial compression tests were carried out on the specimens of group A. During the test, the axial stress was applied to the sample by displacement control at a rate of 0.02 mm/s, and three specimens were repeated at each temperature.

(3) The conventional triaxial compression tests were carried out on the specimens of group B. First, the axial stress and confining pressure were applied simultaneously at the loading rate of 0.5 MPa/s to the preset values (confining pressures were set at 5 MPa, 10 MPa, 15 MPa, 20 MPa and 25 MPa, respectively), then the constant confining pressure was unchanged, the axial direction was changed from force control to displacement control (at a rate of 0.005 mm/s) to apply the axial stress until the specimen was completely destroyed.

4. Analysis of Test Results

4.1. Effect of High Temperature on Longitudinal Wave Velocity of Sample

The Longitudinal wave velocity of two sets of specimens at room temperature (25 °C) and after high temperature are shown in Figure 5. The longitudinal wave velocities are different due to differences in the mineral composition of the two sets of samples. The longitudinal wave velocity of 30 samples in group A is between 3057 and 3630 m/s at room temperature of 25 °C, the average wave velocity is 3277 m/s, and the dispersion coefficient is 3.95%; The longitudinal wave velocity of 25 samples in group B is between 2276 and 2672 m/s at room temperature of 25 °C, the average wave velocity is 2486 m/s, and the dispersion coefficient is 4.41%. It can be seen that although the sample is taken from the same layer, there is still a certain difference in the wave velocity. It may be the existence of pores or fissure in rock that results in the variation of wave velocity of rock samples [28,29]. The ratio

of the maximum difference to the average value of the sample in group A is about 10.8%, and the ratio of the maximum difference to the average value of the sample in group B is about 7.5%. It indicates that the macroscopically homogeneous interior of the sample still exhibits significant heterogeneity.

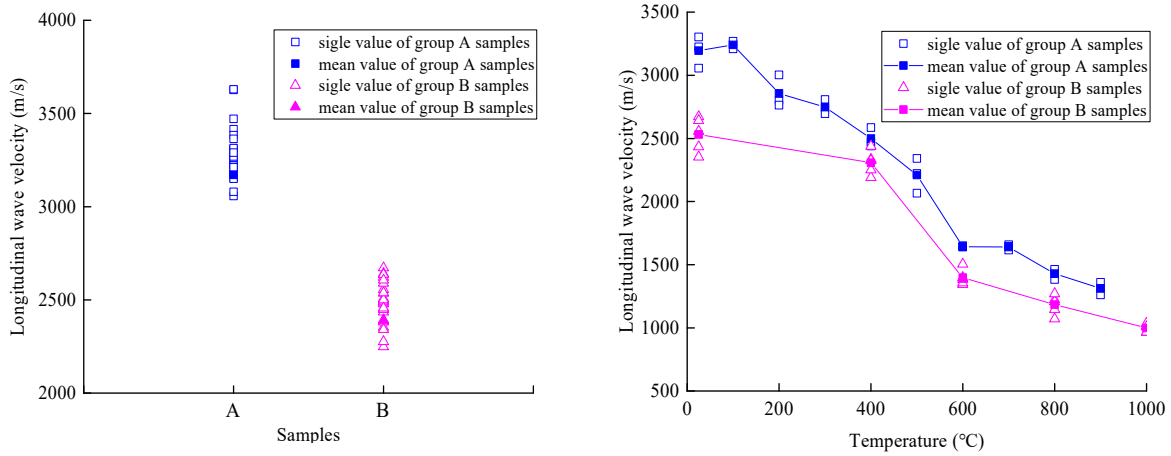

(**a**) Room temperature 25 °C (**b**) After high temperature

Figure 5. Longitudinal wave velocity of two sets of specimens at room temperature 25 °C and after high temperature.

It can be seen from Figure 5 that the longitudinal wave velocities of the samples in group A and B have been reduced to different degrees after different high temperatures. The temperature of 100 °C has little effect on the wave velocity of group A. After 100 °C, the longitudinal wave velocity of the sample decreases linearly with temperature. For group B, the longitudinal wave velocity of group B is nonlinear with temperature increase after high temperature. The high temperature of 400 °C has little effect on the longitudinal wave velocity of the sample in group B, but the effect of high temperature over 400 °C on the longitudinal wave velocity of the sample increases obviously.

After the high temperature action, the structural state and material properties of the sample undergo corresponding physical and mechanical changes, including complex cracks and defects. The ultrasonic waves will undergo refraction and diffraction when they encounter cracks and defects during the propagation process, as a result, the time of penetration of the sample is increased, the wave speed is reduced, and the energy is attenuated. There is a close relationship between the mechanical properties of rock and the longitudinal wave velocity, the longitudinal wave velocity can also indirectly reflect the change of the mechanical properties of the sample after high temperature [30–32]. The damage factor of temperature D can be defined by formula (1), as shown in Figure 6.

$$D = 1 - \left(\frac{V_{pT}}{V_p}\right)^2 \quad (1)$$

where, V_p is the longitudinal wave velocity value of each sample at room temperature 25 °C, m/s; V_{pT} is the longitudinal wave velocity value of each sample after different high temperature, m/s.

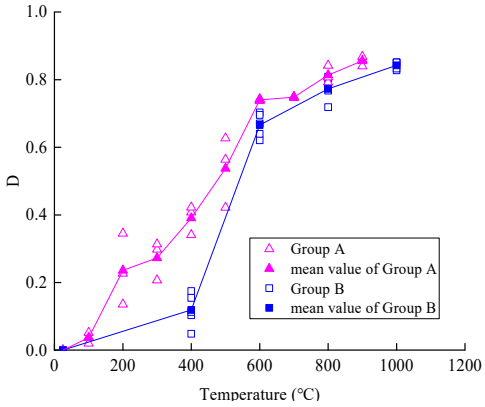

Figure 6. The relationship between damage factors and temperature of high temperature samples.

It can be seen from Figure 6 that the change factors of damage factor and temperature of the two groups are basically the same after high temperature action, and the damage factor becomes larger with the increase of temperature. The damage to the sample is also different due to differences in mineral contents. The damage of the A group is higher than that of the B group. The damage factor of the two groups of samples at 400 °C is 0.42 and 0.13, respectively. When the temperature is at 600~800 °C, the damage factor of the samples is approximately the same. Compared at normal temperature of 25 °C, after 600–800 °C high temperature the damage factors of group A are 0.75 and 0.81, respectively, and the longitudinal damage factors of group B are 0.68 and 0.77, respectively. The reason for this may be that the increase of temperature leads to the increase of porosity and cracks in the sample, which results in the longitudinal wave velocity of the sample to gradually decrease, and the internal damage degree of the sample increase, so that the damage factor of the sample increases with the increase of temperature.

4.2. Analysis of Uniaxial Compression Test Results

4.2.1. Deformation Characteristics

Figure 7 shows the uniaxial compression full stress–strain curves of group A samples after 25 °C, 100 °C, 200 °C, 300 °C, 400 °C, 500 °C, 600 °C, 700 °C, 800 °C and 900 °C. It can be seen from Figure 7 that the variation of the stress–strain curve of the uniaxial compression of the group A samples after different high temperatures generally goes through four stages: compaction, elasticity, yielding and failure.

(1) Compaction: The curve shows upward concave because of the closure of cracks existed under compress. Higher temperatures have long compaction phases, which indicate that the higher the temperature, the more micro-cracks are generated inside the sample.
(2) Elasticity: The stress–strain curve at this stage is a straight line, showing a good linear relationship, showing the elastic characteristics of the material. The slope of the straight line segment at this stage is called the elastic modulus (also known as Young's modulus) and is the mechanical parameter of the material.
(3) Yield: The stress–strain curve bends downward, and the specimen presents inelastic deformation. The material with lower internal strength of the rock specimen first yields and destroys gradually, and the increase rate of axial stress decreases gradually.
(4) Destruction: The axial stress increases to the limit capacity that the specimen can withstand. The micro-cracks inside the specimen penetrate to form a macroscopic slip. In the initial stage of the slip, stress occurs in the longitudinal direction of the specimen, and failure occurs locally [33]. The stress dropped rapidly and the sample as a whole lost its bearing capacity.

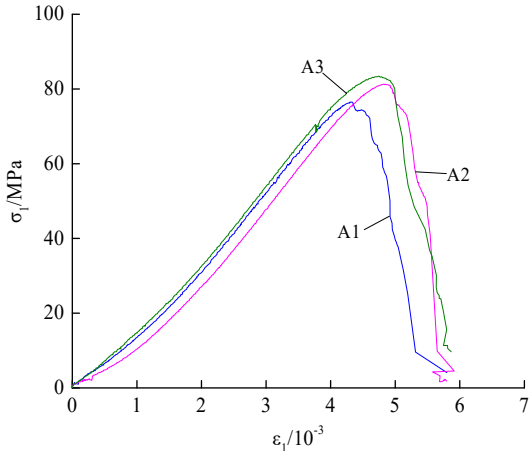

(**a**) 25 °C

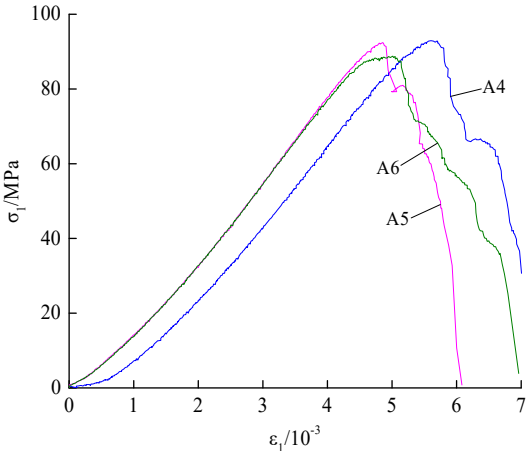

(**b**) 100 °C

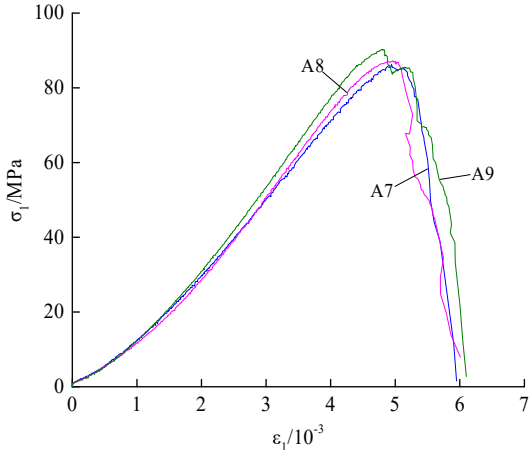

(**c**) 200 °C

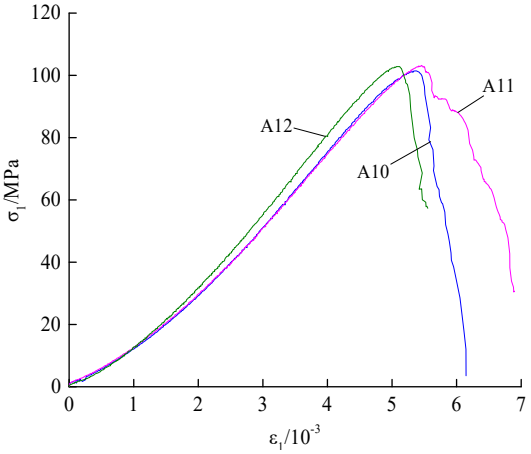

(**d**) 300 °C

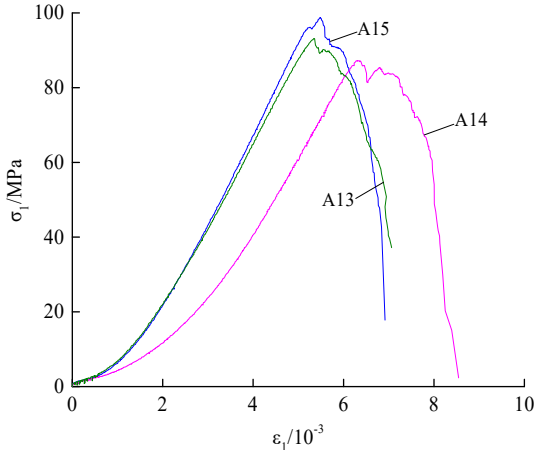

(**e**) 400 °C

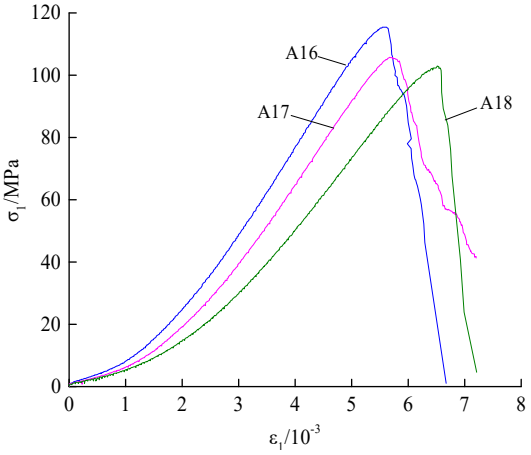

(**f**) 500 °C

Figure 7. *Cont.*

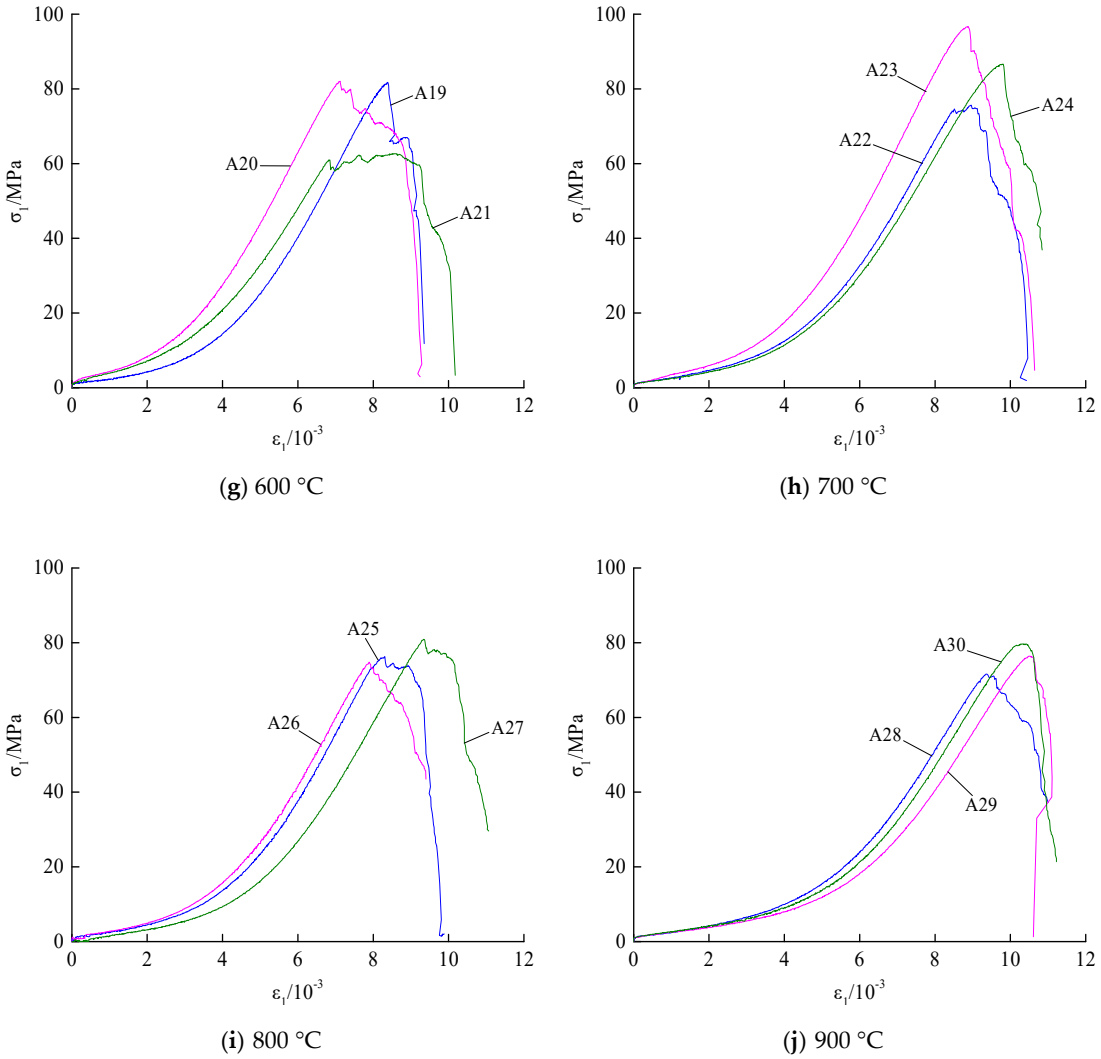

(**g**) 600 °C (**h**) 700 °C

(**i**) 800 °C (**j**) 900 °C

Figure 7. Complete stress–strain curves of samples under uniaxial compression.

For comparison, Figure 8 shows the uniaxial compression of group A samples after 100~900 °C. The stress–strain comparison curve is obtained (one sample at the same temperature).

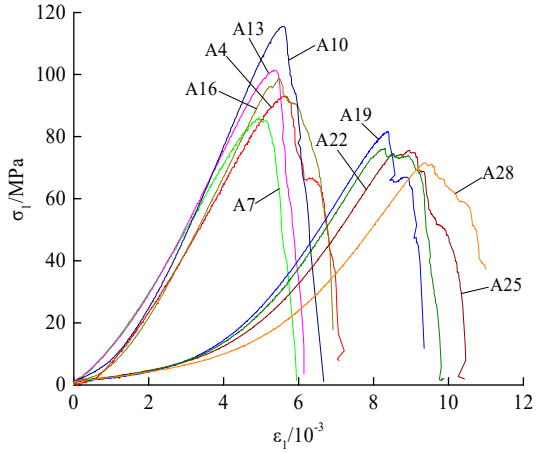

Figure 8. Complete stress–strain curves of one sample at same temperature under uniaxial compression.

It is not difficult to find from Figure 8 that after the sample is subjected to high temperature at 100~500 °C, the four stages of the stress–strain curve deformation process are basically similar, and the elastic modulus is roughly equivalent. It indicates that in this range, the effect of high temperature on the deformation characteristics of the sample during uniaxial compression is not obvious. The effect of high temperature on the bearing capacity of the sample is significant, compared to that at room temperature of 25 °C. Although the test results are largely discrete, they still have obvious general rules, and the bearing capacity of the sample increases with the increase in temperature. This can be explained as being within 500 °C, when the temperature increases, the hot melt deformation can gradually close part of the primary cracks, reduce the number of cracks, improve the contact state between the mineral particles, enhance the friction characteristics, and strengthen the bearing capacity of the sample.

When the temperature exceeds 500 °C, the whole stress–strain curve shape begins to change greatly, which is mainly reflected in the initial resistance to deformation resistance, the stress–strain curve in the compaction phase increases, the stress–strain curve shifts to the right, the peak strain increases significantly, and the bearing capacity decreases. This can be understood as the thermal expansion of the sample mineral particles after the 500 °C high temperature causes the thermal expansion of the grain boundary to be uncoordinated, thereby causing thermal stress between the particles and the thermal stress will produce micro-cracks. At the same time, the decrease of the rigidity will also affect the resistance of the sample to deformation, so that the strength and deformation resistance of the sample are weakened. However, Su et al. [18] considered that 600 °C is the threshold temperature for strengthening and weakening fine sandstone samples. Moreover, as the temperature increases, the intragranular stress further increases, causing the sample to produce micro-cracks or to expand, widen, and connect the primary cracks. Macroscopically, the mechanical properties of the coarse sandstone are degraded, and the peak strength and average modulus of the sample decrease with increasing temperature. Both groups of samples are medium-hard brittle rocks, and the effect of temperature on the post-ductility change is not obvious. The strain showed a softening phase after the peak stress was reached, the stress decreases rapidly, and the strain does not change much, showing brittle failure characteristics.

The relationship between uniaxial compression deformation parameters and temperature of group A samples is shown in Figure 9. Here, it is necessary to specify that the initial modulus E_0, the deformation modulus (secant modulus) E_{50} and the definition are according to the procedure shown in [27]. Elastic modulus (Young's modulus) is E_T. The initial modulus E_0 is the slope of the stress–strain curve passing through the origin in the initial compaction stage. The deformation modulus E_{50} is the slope of the 50% peak intensity connected to the origin of the uniaxial compression axial stress–strain curve. The modulus E_0 and the deformation modulus E_{50} are related to the nonlinear deformation effect in the initial compaction stage of the loading process. The deformation properties of the rock cannot be well characterized. Only the deformation characteristics with stress below 50% of the peak strength can be described. The elastic modulus refers to the slope of the straight line segment on the uniaxial compression axial stress–strain curve; the elastic modulus can characterize the proportional relationship of the stress–strain variation of the material, its value has little effect on the test loading conditions and has a clear mechanical meaning [33]. The peak strain ε_0 represents the strain value corresponding to the peak stress, and the axial compressive strain of the sample consists of the closure of the crack, the slip between the particles, and the elastic strain of the material. The initial stage of the sample loading contains the above three parts. The strain in the elastic and yield stages is mainly composed of the slip between the particles and the elastic compression of the material. The strain in the failure stage is mainly the slip of the macroscopic failure surface.

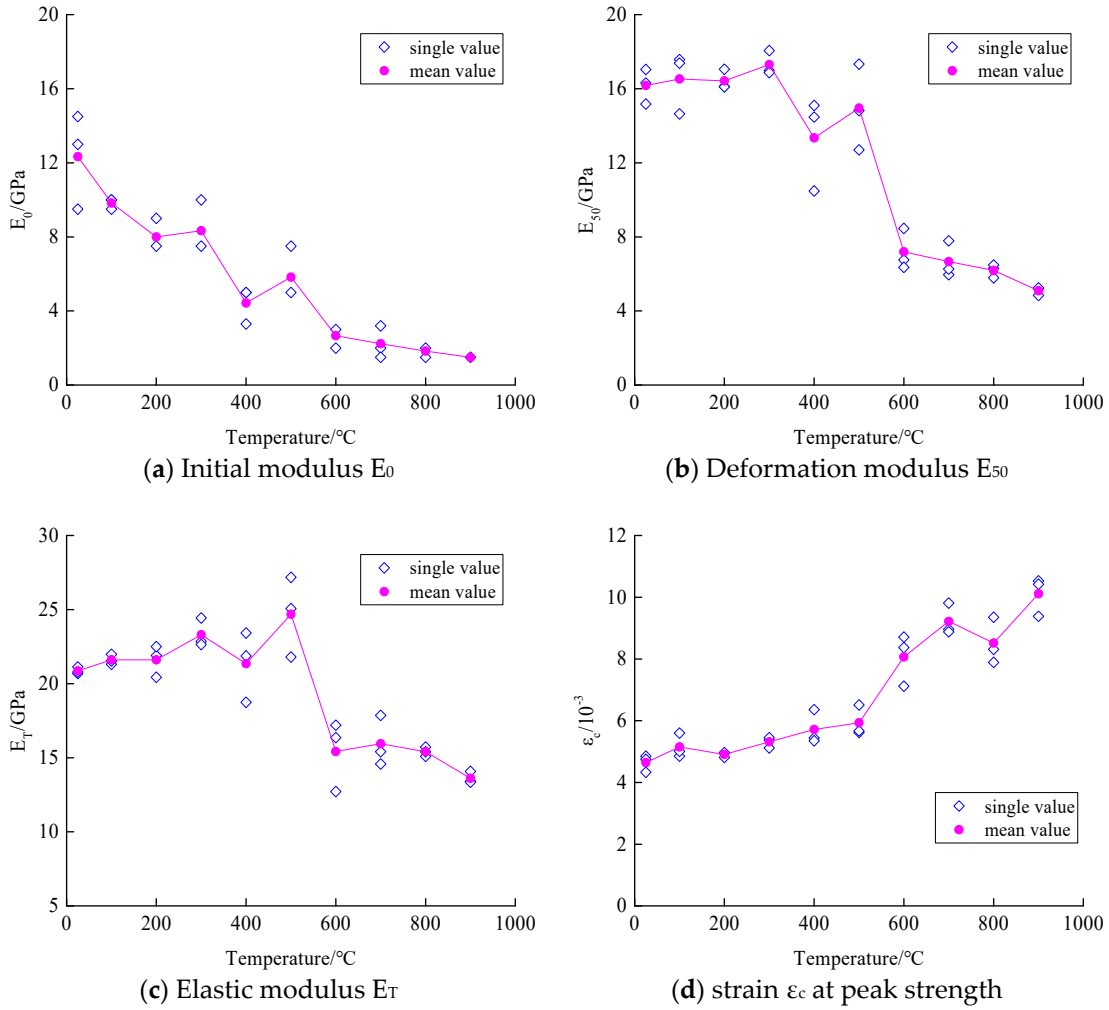

Figure 9. Relationship between uniaxial compressive deformation parameters and temperature.

It can be seen from Figure 9 that the effect of high temperature on the initial modulus E_0, the deformation modulus E_{50}, and the elastic modulus E_T of the sample is not the same. The initial modulus E_0 is particularly affected by high temperature, which is mainly manifested by the fact that the initial stage of loading of the sample is affected by the compaction of the micro-cracks generated by the high temperature. After the high temperature of 100~900 °C, as shown in Figure 9a. Compared with the sample at room temperature of 25 °C, the average modulus E_0 of the sample after 100 °C, 200 °C, 300 °C, 400 °C, 500 °C, 600 °C, 700 °C, 800 °C and 900 °C decreased by 20.3%, 35.1%, 32.4%, 64.0%, 52.7%, 78.4%, 81.9%, and 85.3% respectively.

It can be seen from Figure 9b that the deformation modulus E_{50} of the group A samples increases slightly with the increase of temperature within 300 °C. When the temperature increases from 25 °C to 300 °C, the average deformation modulus increases from 16.17 to 17.3 GPa, the increment is 7%; when the temperature exceeds 300 °C, the deformation parameters of A14 sample is obviously lower, the deformation parameters of A16 sample is obviously higher, and the deformation modulus of other samples decreases sharply with the increase of temperature; The average modulus of deformation of the sample from 500 to 600 °C is reduced from 14.95 to 7.19 GPa with a 50% decrease. The influence of the deformation modulus of the sample in the high temperature range of 600~900 °C is slowed down. Compared with the normal temperature of 25 °C, the average deformation modulus decreased by 52.3%, 55.4%, 58.1% and 64.5 after 600 °C, 700 °C, 800 °C and 900 °C, respectively.

Comparing Figure 9c with Figure 9b, it is not difficult to find that the relationship between deformation modulus, elastic modulus and temperature of group A samples is basically similar after

high temperature action. Compared with the normal temperature of 25 °C, the average elastic modulus of the samples after the high temperatures of 100 °C, 200 °C, 300 °C, 400 °C and 500 °C increased by 3.54%, 3.56%, 11.69%, 2.28% and 18.29%, respectively. When the temperature is raised from 500 to 600 °C, the elastic modulus is greatly reduced, the average elastic modulus is reduced from 24.68 to 15.43 GPa, and the decrease is 37.48%. The elastic modulus of the sample is high in the range of 600~900 °C. The amount of influence is slowed down. Compared to the normal temperature of 25 °C, the average elastic modulus of the samples after 600 °C, 700 °C, 800 °C and 900 °C increased by 26.1%, 23.6%, 26.2% and 34.8%, respectively.

Although the test results are somewhat discrete, it is still possible to show that the average peak strain gradually increases with increasing temperature, and the two are positively correlated; see Figure 9d. After the high temperature of 500 °C, the peak strain of the sample A increased slightly with the increase of temperature. After the high temperature exceeded 500 °C, the peak strain increased rapidly, compared with the normal temperature of 25 °C with peak strain of 4.64×10^{-3}, after 100 After °C, 200 °C, 400 °C, 500 °C, 600 °C, 700 °C, 800 °C and 900 °C, the average peak strain increases by 11.0%, 5.7%, 14.5%, 23.1%, 27.8%, 73.8%, 98.5%, 83.4% and 117.7 %, respectively.

According to the comprehensive analysis, the effect of high temperature on the deformation parameters of group A is significant. The initial modulus E_0 of the sample decreases with the increase of temperature. The longitudinal wave velocity, initial modulus, and temperature of group A are of significantly negative correlation after high temperature; after the high temperature of 500 °C, the elastic modulus, and the peak strain of group A increased, and the deformation modulus of the sample increased slightly within 300 °C; the elastic modulus of group A was higher than 500 °C. The influence of quantity, the deformation modulus and peak strain are significant. The effect of high temperature on the deformation parameters of group A is slowed down by the high temperature of 600~900 °C. The influence of high temperature on the initial modulus and the deformation modulus of the sample is greater than the modulus of elasticity.

4.2.2. Strength Properties

The relationship between uniaxial compressive strength and temperature of samples in group A after different high temperature effects is shown in Figure 10. It can be seen from Figure 10 that the peak intensity of the A21 sample after the high temperature of 400 °C and the high temperature of 600 °C is significantly lower than the peak strength of other samples at the same temperature, which can be understood as the heterogeneity of the sample. Sample dispersion masks the effect of temperature on peak intensity. The compressive strength of the sample increased with the increase of temperature after the high temperature of 500 °C.

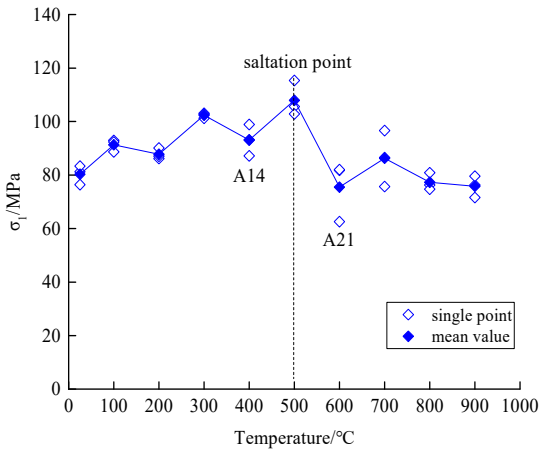

Figure 10. Relationship between uniaxial compressive strength and temperature.

When the temperature exceeded 500 °C, the compressive strength of the sample decreased with the increase of temperature. Compared with the average compressive strength of 80.3 MPa at room temperature of 25 °C, the average compressive strength of group A samples after 100 °C, 200 °C, 300 °C, 400 °C, 500 °C, 600 °C, 700 °C, 800 °C and 900 °C increased by 13.7%, 9.3%, 27.4%, 15.9%, and 34.4%. −6.0%, 7.4%, −3.8% and −5.6%, respectively.

The compressive strengths of the three samples at 500 °C are 115.4 MPa, 105.6 MPa and 102.8 MPa, respectively, and the average compressive strength is 107.9 MPa. The high temperature effect in the range of 100~500 °C was observed, the ability has a strengthening effect. The high temperature action of more than 500 °C slightly reduces the bearing capacity of the sample, which is roughly equivalent to the peak intensity of 25 °C at room temperature, which indicates that the high temperature effect at 900 °C has no obvious influence on the uniaxial compressive strength of the sample.

4.2.3. Failure Patterns

The failure mode of the uniaxial compression of the sample after different high temperature is shown in Figure 11. The uniaxial compression failure of the sample is more complicated. Most of the failure modes of the sample are single diagonal shear failure, and the crack is applied to the edge of the end of the sample. In the sample, most of the shear plane starts at the edge of the end face of the specimen, but the projection of the entire shear plane in the horizontal plane covers the entire section of the specimen, and the X-shaped conjugate shear of the specimen occurs due to the friction effect of the upper and lower ends. The individual samples are conical, as shown in Figure 11a for A1 and Figure 11b for A5. The main shear fracture surface has powdery substances with obvious friction marks and some samples appear. The longitudinal crack is parallel to the loading direction, as shown in Figure 11b for the A6 sample and Figure 11h for the A24 sample, and the failure mode of the sample becomes more complicated with the increase of temperature. The higher the temperature is, the more severe the damage of the sample and the increase of the detached powdered sand will be.

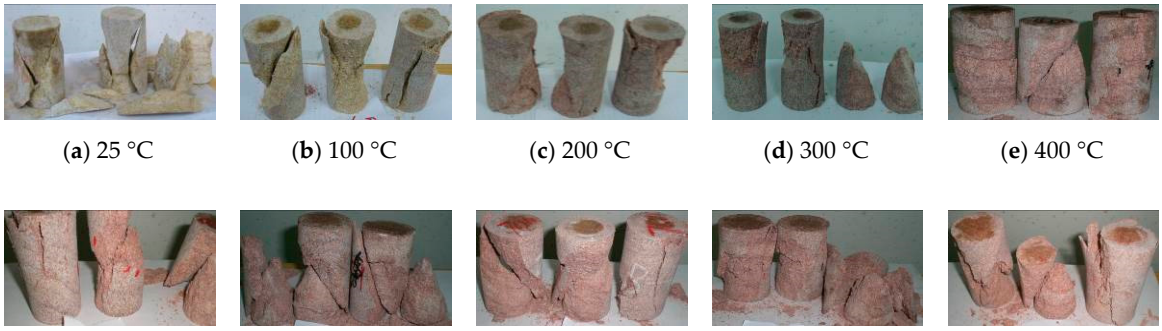

(**a**) 25 °C (**b**) 100 °C (**c**) 200 °C (**d**) 300 °C (**e**) 400 °C

(**f**) 500 °C (**g**) 300 °C (**h**) 700 °C (**i**) 800 °C (**j**) 900 °C

Figure 11. Uniaxial compression failure modes after high temperature.

4.3. Analysis of Triaxial Compression Test Results

4.3.1. Deformation Properties

The complete stress–strain curve of the triaxial compression test of the B group samples after the high temperature action is shown in Figure 12. It can be seen from Figure 12 that the regular triaxial compression stress–strain curve of the sample after the high temperature action is basically the same as that of Figure 7, and is roughly divided into four stages: compaction, elasticity, yielding, and failure. The deformation characteristics of the specimens are different under the action of temperature and confining pressure, and the axial compression deformation increases with the increase of temperature.

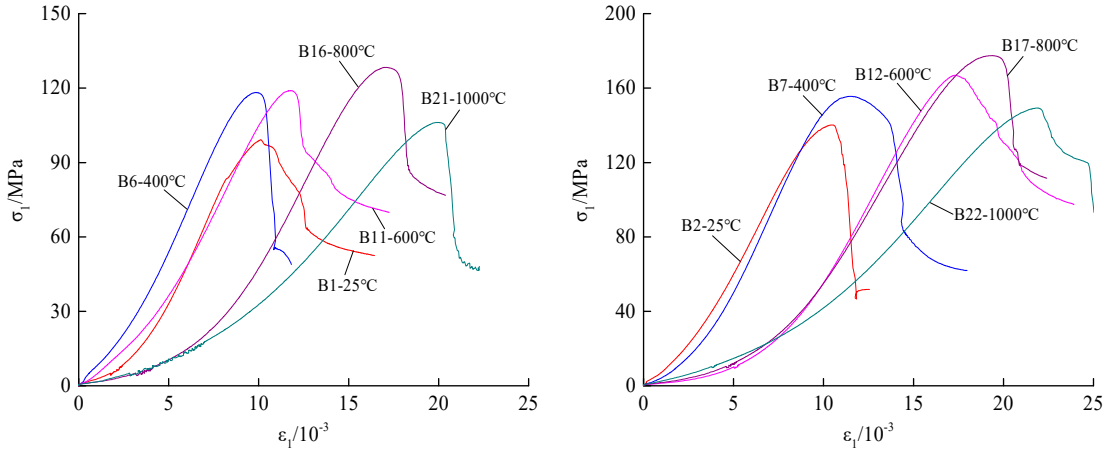

(**a**) 5 MPa (**b**) 10 MPa

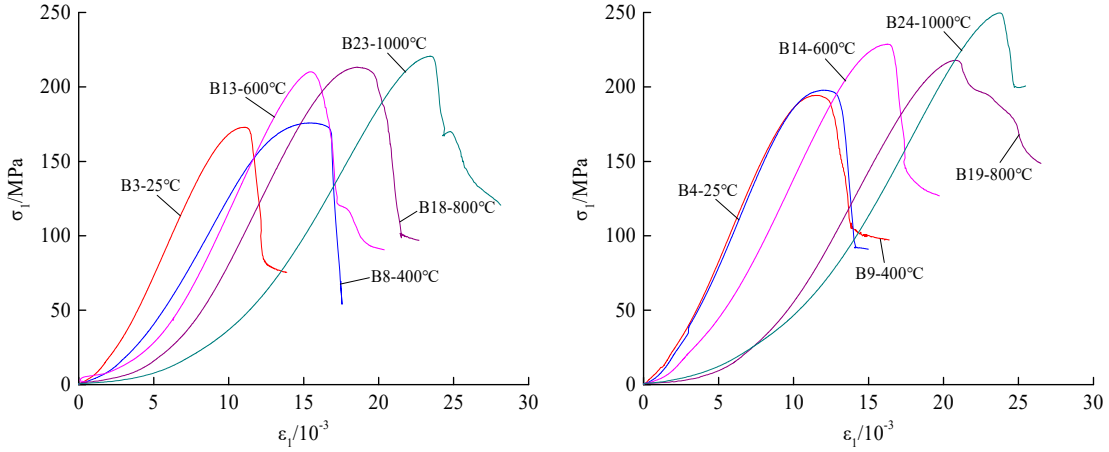

(**c**) 15 MPa (**d**) 20 MPa

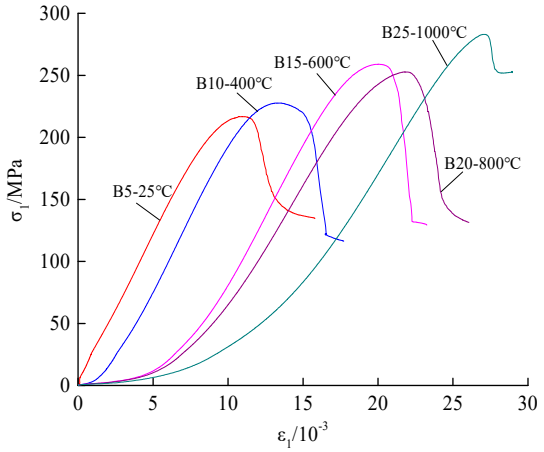

(**e**) 25 MPa

Figure 12. Complete stress–strain curve of samples after high temperature under conventional triaxial compression condition.

Under the action of confining pressure of 5~25 MPa, the initial compaction phases of loading are obvious, and the higher temperature of the specimen is, the longer the compaction phases is. For

example, in Figure 12e, after the 1000 °C high temperature effect, the densification of the B25 specimen is still obvious under the action of confining pressure of 25 MPa, and the initial nonlinear deformation is mainly dominated by crack closure. The elastic phase is mainly the elastic deformation of the mineral particles. The yield phase is mainly composed of inter-particle slip, elastic deformation, and yield deformation. The destruction phase is mainly macroscopic fissure slip and friction. Of course, the strength of the cement will decrease and the inter-particle slip will increase when specimen passes through a higher temperature.

Under the same confining pressure, the relation between deformation parameters and temperature after different high temperature are shown in Figure 13. Compared with the results of the normal 25 °C test, the effect of high temperature within 400 °C has little effect on the deformation parameters. Once the temperature exceeds 400 °C, the impact on the elastic modulus, deformation modulus, and peak strain is greater. Although the sample is affected by its own heterogeneity, the test results are some discrete, and the high temperature still has some regularity effect on the specimen deformation parameters: the elastic modulus and the deformation modulus decreased monotonically with increasing temperature, and peak strain increased monotonically with increasing temperature. Compared with the normal 25 °C test results, after 600 °C, 800 °C and 1000 °C high temperature, the increase of elastic modulus by an average of −8.26%, −15.30% and −33.30%, respectively; the decrease of deformation modulus by an average of −18.60%, −28.29% and −47.33%, respectively; and the increase of axial strain in perk strength by an average of 48.41%, 79.57% and 113.21%, respectively.

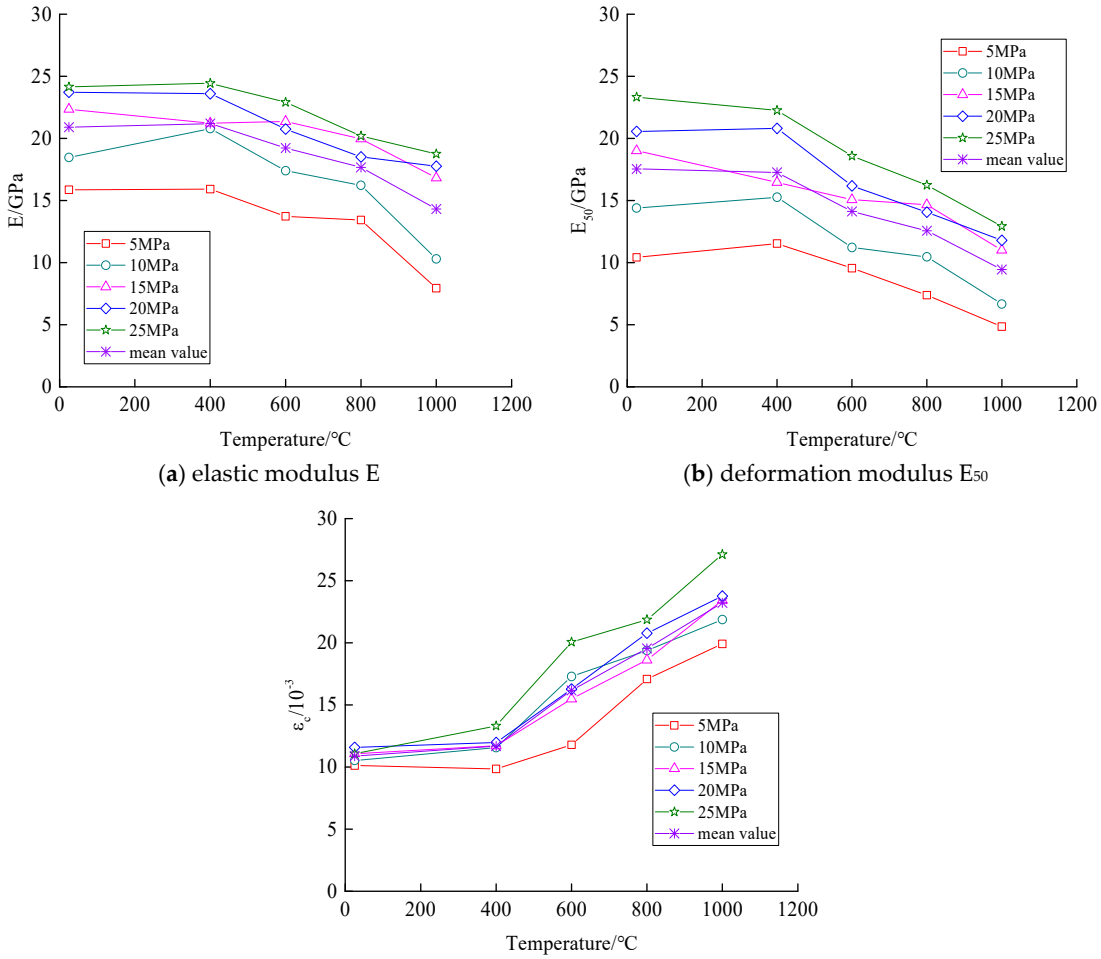

(**a**) elastic modulus E

(**b**) deformation modulus E_{50}

(**c**) axial strain ε_c at peak strength

Figure 13. Relationship between temperature and deformation parameters of triaxial compression test.

The above analysis shows that the high temperature effect within 400 °C has little effect on the deformation parameters of group B samples. Once the temperature exceeds 400 °C, the elastic modulus, deformation modulus and confining pressure of the sample are linearly positively correlated with temperature. There is a linear negative correlation and the peak strain is positively correlated with the confining pressure and temperature.

4.3.2. Strength Properties

Figure 14 shows the relationship between the three axis strength and the confining pressure and temperature after high temperature. From Figure 14a, it can be seen that the peak strength of the triaxial compression test of group B is approximately linear with the confining pressure after high temperature, and this conforms to the Coulomb strength criterion.

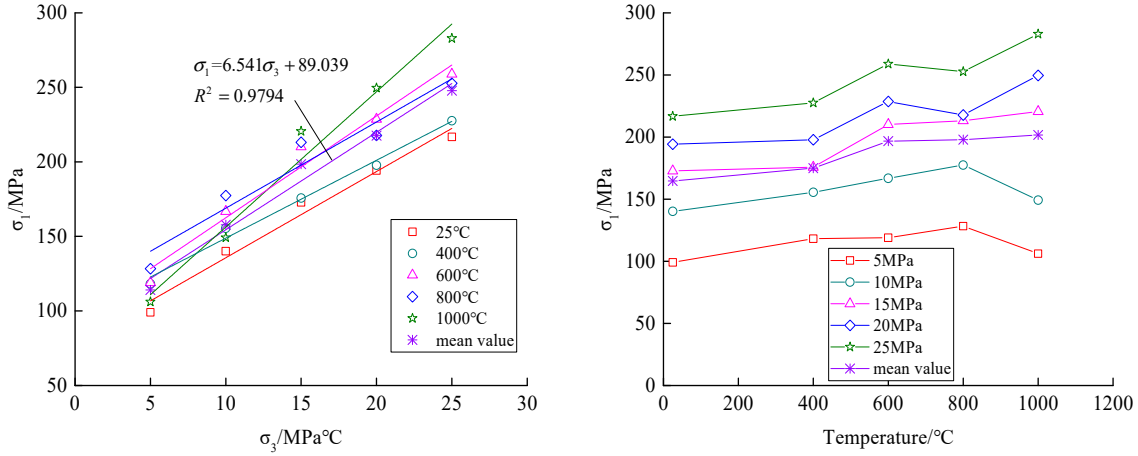

(**a**) strength and confining pressure (**b**) strength and temperature

Figure 14. Relationship between three axis strength and confining pressure and temperature after high temperature.

According to Coulomb strength criterion:

$$\sigma_1 = k\sigma_3 + Q \tag{2}$$

In the formula, Q and k are the material parameter.

According to Equation (2), the relationship between the triaxial strength and the confining pressure is obtained, as shown in Table 1. After the high temperature of 800 °C, the influence coefficient k of the sample is about 5.233~6.833, which indicates that the high temperature of 800 °C has little effect on the confining pressure influence coefficient k of the sample. After 1000 °C , the influence coefficient k of the sample confining pressure increased significantly, reaching 9.078. From the fitting correlation of the test results of the samples after different high temperature, except for the low correlation coefficient of the sample after 800 °C high temperature; and the other fitting correlation coefficients are greater than 0.973. The axial strength has a good linear correlation with the confining pressure, which is in accordance with the Coulomb strength criterion. The comprehensive confining pressure influence coefficient is 6.541 and the correlation coefficient is 0.979.

Table 1. Strength characters of samples under conventional triaxial compression after temperature.

T/°C	*k*	*Q*/MPa	R^2
25	5.786	77.80	0.979
400	5.233	96.61	0.989
600	6.833	94.17	0.973
800	5.784	111.20	0.940
1000	9.078	65.61	0.975

Figure 14b shows that the peak intensity of the triaxial compression is almost the same under the confining pressure conditions when the temperature is lower than 800 °C; that is, the peak intensity increases as the temperature increases. When the temperature exceeds 800 °C, the sample shows two different development trends: under low confining pressure (5 MPa, 10 MPa), the peak strength decreases with increasing temperature; under high confining pressure (20 MPa, 25 MPa), the peak intensity increases with the increase of temperature; while under the medium confining pressure (15 MPa), the peak intensity is weakly changed by temperature, showing a transitional sign.

The Strength of the specimen depends on the bonding and friction based on Coulomb strength theory. However, the melting and disappearance of the fusible material inside the specimen at high temperature causes the micro-crack to increase, which will inevitably lead to the change of the cohesive force of the sample. The influence of particle size is very weak, and the roughness of the sample does not change qualitatively. Therefore, for Equation (2), the *k* value should be a fixed value, and *Q* can be understood as a uniaxial compressive strength at the time of shear failure of the uniaxial compression of the complete sample (the confining pressure is 0 MPa), which can be regarded as the material strength.

Figure 15 shows the relationship between the strength of the sample material and the temperature and confining pressure after deducting the confining pressure after high temperature.

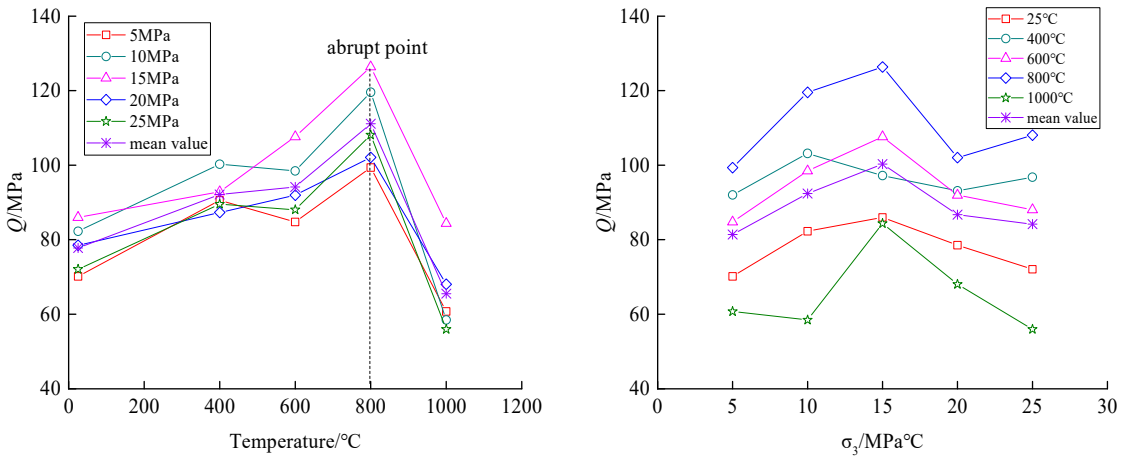

Figure 15. The relationship between the strength of material and temperature and confining pressure.

It can be seen from Figure 15 that although the sample is affected by its own heterogeneity, the test results are somewhat discrete. The measured material strength and temperature change trend are basically the same under different confining pressures, at room temperature of 25 °C and after 400, 600, 800, and 1000 °C, the average material strength *Q* after deducting the confining pressure is 77.8, 92.1, 94.2, 111.1, and 65.5 MPa, respectively. The high temperature of 800 °C has a strengthening effect on the sample. After deducting the confining pressure, the sample material strength *Q* is positively correlated with the temperature. When the temperature exceeds 800 °C, the high temperature effect has a degrading effect on the sample, and the material strength *Q* is negatively correlated with the temperature (as shown in Figure 15a). After 400~600 °C high temperature effect on the material strength

is roughly equivalent, after 800 °C high temperature effect on the material strength has been greatly improved, after the 1000 °C high temperature effect, the material strength decreased sharply, while at 800 °C, material strength showed a sudden change. Compared with the normal temperature of 25 °C, the average increase of sample material strength after 400, 600, 800, and 1000 °C high temperature is 18.87%, 20.99%, 42.78%, and −15.98%.

The relationship between material strength and confining pressure under different temperature conditions is shown in Figure 15b. The average material strength increases with the increase of confining pressure at 25 °C and high temperature. When the confining pressure is lower than 15 MPa, the material strength increases with confining pressure. When the confining pressure is higher than 15 MPa, the strength of the material decreases, and the strength of the material with a confining pressure of 15 MPa is abrupt. Compared with the material strength at room temperature, the strength of the material increased after 400, 600, and 800 °C high temperature, and the strength of the material decreased after 1000 °C high temperature. That is to say, under the condition that the temperature is lower than 800 °C and the confining pressure is lower than 15 MPa, the material strength is positively correlated with temperature and confining pressure. When the temperature exceeds 800 °C and the confining pressure is higher than 15 MPa, the material strength, temperature, and confining pressure are negatively correlation, indicating that temperature and confining pressure conditions have an impact on the strength of the sample material, 800 °C is the temperature threshold, and 15 MPa is the confining pressure threshold.

4.3.3. Failure Patterns

Figure 16 shows the fracture morphology of group B samples after triaxial compression after high temperature action. Compared with the failure mode of the uniaxial compression test in Figure 11, the damage mode in the triaxial compression test is relatively simple, and most of them are typical shear failures, it is likely to be due to the presence of a confining pressure. The shear surface of the individual samples is conical, and the main shear fracture surface has fine powdery substances with obvious friction marks. Most of the shear plane starts at the edge of the end face of the specimen, and the individual specimens are cracked at the end of the specimen. The projection of the entire shear plane in the horizontal plane covers the cross section of the whole sample, and a few horizontal cracks perpendicular to the loading direction appear on the shear surface of a few specimens. For example, in Figure 16, the B8 sample under the action of confining pressure 15 MP after 400 °C high temperature and the B12 sample under the action of confining pressure 10 MP after 600 °C high temperature may cause the main rupture surfaces slip each other and a horizontal force causes the slip block to break laterally.



(**a**) 25 °C (**b**) 400 °C (**c**) 600 °C

(**d**) 800 °C (**e**) 1000 °C

Figure 16. Rupture morphology of samples under conventional compression condition after high temperature.

Figure 17 shows the relationship between the fracture angle of the sample, the temperature, and confining pressure after the high temperature action. Although the sample is affected by its own heterogeneity, the test results are somewhat discrete. The triaxial compression fracture angle of the sample under different temperature and confining pressure fluctuates. At high temperatures, the actual fracture angle of the sample is consistent with the theoretical calculation value. The effect on the fracture angle of the sample is small, and the fracture angle of the sample increases slightly as the temperature increases, as shown in Figure 17a. Compared with the actual rupture angle of 64.6° at room temperature of 25 °C, the average actual rupture angles of the samples after 400, 600, 800, 1000 °C is 64.6, 63.0, 66.6, 66.0, and 67.7°, the increase rate is −2.5%, 3.1%, 2.2%, and 4.6%, respectively; according to Coulomb strength criterion theory, the fracture angle (45° + φ/2), is 67.5, 66.4, 69.1, 67.4, and 71.7, the average actual rupture angle of the visible sample is less than the theoretical calculated rupture angle of 1.4°~4.1°. This can explain the friction effect of the sample on the upper and lower end heads. During the compression of the sample, the axial compression of the sample is laterally expanded, while the stiffness of the upper and lower end heads is much larger than the stiffness of the sample, which restricts the lateral expansion of the sample to produce friction, thereby affecting the crack propagation at the end of the sample, so that the actual cracking and outward rupture angle becomes small.

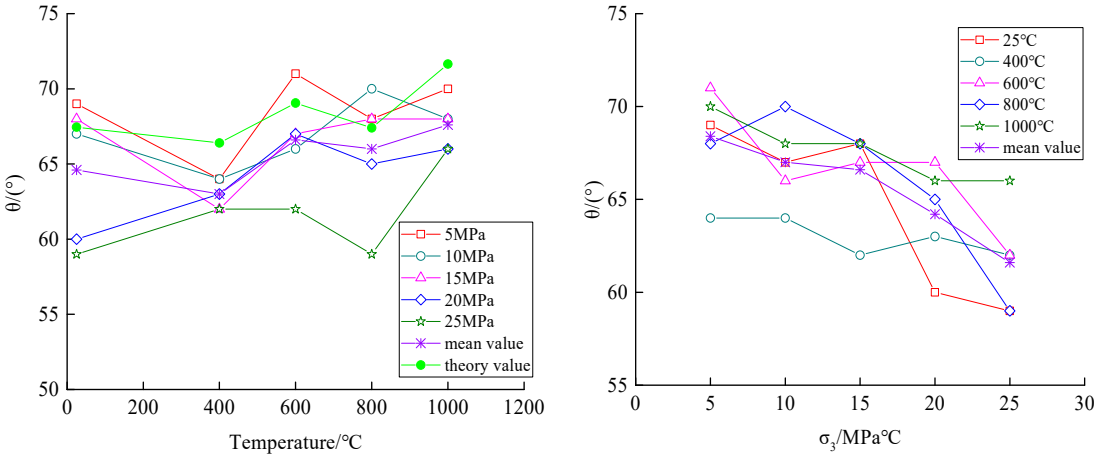

(**a**) fracture angle and temperature (**b**) fracture angle and confining pressure

Figure 17. Relationship between three axis strength and confining pressure and temperature after high temperature.

Figure 17b shows that the actual fracture angle of the sample is negatively correlated with the confining pressure after the high temperature action, and the actual fracture angle monotonously decreases with the increase of the confining pressure. Compared with the actual rupture angle of 68.4° of 5 MPa, the average rupture angles of the specimens under the confining pressures of 10, 15, 20, and 25 MPa is 67, 66.6, 64.2, and 61.6°, with a decrease of 2.04%, 2.63%, 6.14%, and 9.94%, respectively. It shows that the influence of confining pressure on the fracture angle of the sample is greater than the influence of temperature.

5. Discussion

After experiencing different temperatures, the uniaxial compressive strength, average modulus, modulus of deformation, initial modulus, ultimate strain, and longitudinal wave velocity of coarse sandstone samples show that the high temperature effect has a certain influence on the physical and mechanical parameters of coarse sandstone. Since the coarse sandstone sample is a heterogeneous anisotropic body, the test results are scattered widely, but there are obvious rules on the whole. For uniaxial compression, the load-bearing capacity and deformation resistance of the specimen are

strengthened when the temperature is less than 500 °C. Compared with the room temperature of 25 °C, the strength, average modulus and peak deformation of the specimen are improved in varying degrees. When the temperature exceeds 500 °C, the average strength increases by 34%, the average modulus increases by 17.4%, the peak deformation increases by 27.8%, the deformation modulus decreases slightly by 7.5%, especially the wave velocity, which decreases by 53%.

The coarse sandstone sample is a kind of high-porosity rock. The rock particles are not very compact, and there are more pores and fissures between them. These larger pore structures can accommodate deformation and prevent crack propagation when the temperature is lower than 500 °C. The thermal expansion of mineral particles may also cause the primary cracks in coarse sandstone sample to close gradually, and the number of cracks decreases, the internal compactness of the sample is improved. When the temperature decreases, the contact relationship between mineral particles can be improved, the friction characteristics can be enhanced, and the load-bearing capacity and anti-deformation ability of the samples can be strengthened.

When the temperature exceeds 500 °C, the different thermal expansion rates of the mineral particles inside the coarse sandstone sample cause the inconsistency among particles, which makes the mineral particles or within particles, i.e., structural thermal stress. Once the structure thermal stress reaches or exceeds the ultimate strength of the material, micro-cracks will occur, which will weaken the bearing capacity and deformation resistance of the coarse sandstone sample. With the increase of temperature, the inter-particle stress will further increase, resulting in produce more micro-cracks in the coarse sandstone sample, or the expansion, broadening and connection of primary cracks. At the same time, the reduction of the rigidity of the cements will also affect the deformation of the sample. Macroscopically, the mechanical properties of the coarse sandstone will deteriorate, and the bearing capacity and deformation resistance of the sample will decrease. It can be seen that the threshold temperature of mechanical parameters of coarse sandstone is 500 °C.

6. Conclusions

In this paper, we carried out uniaxial compression and triaxial compression tests of two sets of samples by applying a temperature of 25 °C and a high temperature of 100~1000 °C, and obtained some meaningful conclusions. The research results can provide some reference and help for the development of engineering design and high temperature rock mechanics theory.

(1) With the increase of temperature, the longitudinal wave velocity gradually decreases, and the damage factor of temperature gradually increases.
(2) For uniaxial compression tests at different temperatures, the high temperature action within 500 °C has a strengthening effect on the compression strength, and the high temperature effect has a weakening effect on the compression strength exceed 500 °C, so 500 °C is the temperature threshold.
(3) For triaxial compression tests at different temperatures, the rock strength is positively correlated with temperature and confining pressure when the temperature is lower than 800 °C and the confining pressure is lower than 15 MPa; the rock strength is negatively correlated with temperature and confining pressure when the temperature is over 800 °C and confining pressure is above 15 MPa, so 800 °C is the temperature threshold, and 15 MPa is the confining pressure threshold.
(4) In the triaxial compression, the actual fracture angle of the sample at high temperatures is basically the same as the theoretical calculation value, the high temperature has little effect on the actual fracture angle of the sample, and the actual fracture angle is negatively correlated with the confining pressure.

Author Contributions: S.W. supervised the research. Y.Y. and C.S. helped in writing and re-checking the paper technically as well as figures and texts. S.R.C. and H.W. polished the English of the paper.

Funding: This work was supported by National Natural Science Foundation of China (No. 51674101), Key Scientific and Technological Research Projects in Henan Province (182102210317), Funding Project of Fundamental Research Business Expenses of Universities in Henan Province (NSFRF180402).

Conflicts of Interest: The authors declare no conflict of interest.

References

1. He, G.L.; Wu, G.; Huang, X.C.; Zhang, L.; Qiu, Y.P. Experimental study on ultrasonic properties of sandstone before and after high temperature. *Rock Soil Mech.* **2007**, *28*, 779–784.
2. Zuo, J.P.; Zhou, H.W.; Liu, Y.J. Research on characteristic parameters of sandstone three-point bending failure under different temperatures. *Chin. J. Rock Mech. Eng.* **2010**, *29*, 705–712.
3. Zuo, J.P.; Xie, H.P.; Liu, Y.J. Investigation on fracture characteristics of sandstone after thermal effects through three-bending point experiments. *Chin. J. Solid Mech.* **2010**, *31*, 119–126.
4. Wu, G.; Xing, A.G.; Zhang, L. Mechanical characteristics of sandstone after high temperature. *Chin. J. Rock Mech. Eng.* **2007**, *26*, 2110–2116.
5. Wu, G.; Wang, Y.; Zhai, S.T. Acoustic emission characteristics of sandstone after high temperature under uniaxial compression. *Rock Soil Mech.* **2012**, *33*, 3237–3242.
6. Wu, G.; Zhai, S.T.; Wang, Y. Research on characteristics of mesostructure and acoustic emission of granite under high temperature. *Rock Soil Mech.* **2015**, *36*, 351–356.
7. You, M.Q.; Su, C.D.; Li, X.S. Study on relation between mechanical properties and longitudinal wave velocities for damaged rock samples. *Chin. J. Rock Mech. Eng.* **2008**, *27*, 458–467.
8. Chen, Y.L.; Ni, J.; Shao, W.; Azzam, R. Experimental study on the influence of temperature on the mechanical properties of granite under uni-axial compression and fatigue loading. *Int. J. Rock Mech. Min. Sci.* **2012**, *56*, 62–66. [CrossRef]
9. Brotóns, V.; Tomás, R.; Ivorra, S.; Alarcon, J.C. Temperature influence on the physical and mechanical properties of a porous rock: San Julian's calcarenite. *Eng. Geol.* **2013**, *167*, 117–127. [CrossRef]
10. Huang, S.; Xia, K.W. Effect of heat-treatment on the dynamic compressive strength of Longyou sandstone. *Eng. Geol.* **2015**, *191*, 1–7. [CrossRef]
11. Xu, X.L.; Gao, F.; Zhang, Z.Z.; Chen, L. Experimental study of the effect of loading rates on mechanical properties of granite at real-time high temperature. *Rock Soil Mech.* **2015**, *36*, 2184–2192.
12. Yao, W.; Xu, Y.; Wang, W.; Kanopolous, P. Dependence of Dynamic Tensile Strength of Longyou Sandstone on Heat-Treatment Temperature and Loading Rate. *Rock Mech. Rock Eng.* **2015**, *49*, 3899–3915. [CrossRef]
13. Yu, J.; Chen, X.; Li, H.; Zhou, J. Effect of freeze-thaw cycles on mechanical properties and permeability of red sandstone under triaxial compression. *J. Mt. Sci.* **2015**, *12*, 218–231. [CrossRef]
14. Chmel, A.; Shcherbakov, I. Microcracking in impact-damaged granites heated up to 600 degrees C. *J. Geophys. Eng.* **2015**, *12*, 485–491. [CrossRef]
15. Geng, J.S.; Sun, Q.; Zhang, W.Q.; Lü, C. Effect of high temperature on mechanical and acoustic emission properties of calcareous-aggregate concrete. *Appl. Therm. Eng.* **2016**, *106*, 1200–1208. [CrossRef]
16. Huang, Z.P.; Zhang, Y.; Wu, E.D. Analysis of mechanical and wave properties of heat-treated marble by water cooling. *Rock Soil Mech.* **2016**, *37*, 367–375.
17. Su, C.D.; Wei, S.J.; Qin, B.D.; Yang, Y.S. Experimental study of influence mechanism of high temperature on mechanical properties of fine-grained sandstone. *Rock Soil Mech.* **2017**, *38*, 623–630.
18. Su, C.D.; Guo, W.B.; Li, X.S. Experimental research on mechanical properties of coarse sandstone after high temperatures. *Chin. J. Rock Mech. Eng.* **2008**, *27*, 1162–1170.
19. Ma, J.H.; Wei, S.J.; Su, C.D. Effect of high temperature on the mechanical properties of the sandstone physical weak bond. *J. Min. Saf. Eng.* **2017**, *34*, 155–162.
20. Huang, Y.H.; Yang, S.Q. The tensile mechanical behavior of granite containing pre-existing holes after high temperature treatment. *J. China Univ. Min. Technol.* **2017**, *46*, 783–791.
21. Shao, Z.S.; Wu, K.; Yuan, Y. Theoretical investigation on rock rheological characteristics in variable temperature field. *Chin. J. Appl. Mech.* **2018**, *35*, 962–969.
22. Li, E.B.; Wang, Y.C.; Chen, L.; Liu, Y. Experimental study of mechanical properties of Beishan granite's thermal damage. *J. China Univ. Min. Technol.* **2018**, *47*, 735–741.
23. Kong, B.; Wang, E.Y.; Li, Z.H.; Wang, X.R.; Niu, Y.; Kong, X.G. Acoustic emission signals frequency-amplitude characteristics of sandstone after thermal treated under uniaxial compression. *J. Appl. Geophys.* **2017**, *136*, 190–197. [CrossRef]

24. Becattini, V.; Motmans, T.; Zappone, A.; Madonna, C.; Haselbacher, A.; Steinfeld, A. Experimental investigation of the thermal and mechanical stability of rocks for high-temperature thermal-energy storage. *Appl. Energy* **2017**, *203*, 373–389. [CrossRef]
25. Zhang, D.M.; Yang, Y.S.; Yang, H.; Chu, Y.P.; Yang, S. Experimental study on the effect of high temperature on the mechanical properties and acoustic emission characteristics of gritstone. *Results Phys.* **2018**, *9*, 1609–1617. [CrossRef]
26. Ersoy, H.; Hasan Kolayli, H.; Karahan, M.; Karahan, H.; Sünnetci, M.O. Effect of thermal damage on mineralogical and strength properties of basic volcanic rocks exposed to high temperatures. *Bull. Eng. Geol. Environ.* **2019**, *78*, 1515–1525. [CrossRef]
27. Coal Industry Ministry of the People's Republic of China. *Measuring Methods of Physico-Mechanical Properties for Coal and Rock*; Standards Press of China: New York, NY, USA, 1988; pp. 32–33.
28. Kahraman, S.; Yeken, T. Determination of physical properties of carbonate rocks from P-wave velocity. *Bull. Eng. Geol. Environ.* **2008**, *67*, 277–281. [CrossRef]
29. Pappalardo, G.; Mineo, S.; Monaco, C. Geotechnical characterization of limestones employed for the reconstruction of a UNESCO world heritage Baroque monument in southeastern Sicily (Italy). *Eng. Geol.* **2016**, *212*, 86–97. [CrossRef]
30. Pappalardo, G.; Punturo, R.; Mineo, S.; Contrafatto, L. The role of porosity on the engineering geological properties of 1669 lavas from Mount Etna. *Eng. Geol.* **2017**, *221*, 16–28. [CrossRef]
31. Torok, A.; Vasarhelyi, B. The influence of fabric and water content on selected rock mechanical parameters of travertine, examples from Hungary. *Eng. Geol.* **2010**, *115*, 237–245. [CrossRef]
32. Tugrul, A.; Zarif, I.H. Engineering aspects of limestone weathering in Istanbul, Turkey. *Bull. Eng. Geol. Environ.* **2000**, *58*, 191–206. [CrossRef]
33. You, M.Q. *Mechanical Properties of Rocks*; Geological Publishing House: Beijing, China, 2007; pp. 25–26.



© 2019 by the authors. Licensee MDPI, Basel, Switzerland. This article is an open access article distributed under the terms and conditions of the Creative Commons Attribution (CC BY) license (http://creativecommons.org/licenses/by/4.0/).